Tribological Testing of Peroxide Cured HNBR with Different MWCNT and Silica Contents under Dry Sliding and Rolling Conditions Against Steel

D. Felhös, J. Karger-Kocsis, D. Xu

Institut für Verbundwerkstoffe GmbH (Institute for Composite Materials), Kaiserslautern University of Technology, Kaiserslautern D-67663, Germany

Received 7 May 2007; accepted 3 November 2007
DOI 10.1002/app.27624
Published online 25 February 2008 in Wiley InterScience (www.interscience.wiley.com).

ABSTRACT: The sliding, and rolling friction and wear behaviors of peroxide cured hydrogenated nitrile rubber (HNBR) with 10 and 30 parts per hundred rubber (phr) multiwall carbon nanotube (MWCNT) and silica, respectively, were investigated. Mechanical properties (hardness, tensile modulus, ultimate tensile strength and strain, tear strength) of the rubbers were determined. Dynamic-mechanical thermal analysis was also performed and the apparent crosslink density estimated. Tribological properties were investigated in pin (steel)-on-plate (rubber), with roller (steel)-on-plate (rubber), with oscillating steel cylinder on rubber plate (Fretting) and with rolling ball (steel)-on-plate (rubber) (RBOP) test configurations. Coefficient of friction and specific wear rate (Ws) of the HNBR systems were determined. It was established that the resistance to wear increases with increasing filler content, and the incorporation of MWCNT was more advantageous than silica from the viewpoint of dry sliding and rolling performance. The friction and wear characteristics strongly depended on the test configurations. The worn surface of the HNBR systems was inspected in scanning electron microscope to conclude the typical wear mechanisms which were discussed accordingly. © 2008 Wiley Periodicals, Inc. J Appl Polym Sci 108: 2840–2851, 2008

Key words: nanocomposites; reinforcement; rubber; silicas; carbon nanotube; wear

INTRODUCTION

Rubbers are widely used as constructional and engineering materials in various fields, such as automotive industry (tire, sealing), building and construction (roofing, dilatational joint). Rubbers are indispensable materials also for mechanical engineering applications (e.g. pneumatic or hydraulic sealing, damping elements). The broad application of rubbers is due to their low modulus, extremely large reversible deformability, and high internal damping. Owing to this unique property combination, which can even be tailored upon request, rubbers are the first choice materials for damping and sealing elements. Their demanding property profile can be met with new rubber recipes which often contain novel fillers. Such new fillers are, for example, organoclays and carbon nanotubes (CNT). When exfoliated, i.e. becoming nanoscale dispersed, these fillers upgrade the stiffness, strength, and other properties (e.g. barrier and flame resistance) of the corresponding rubbers. Organoclays and CNTs were already incorporated in various polymers in order to improve their mechanical properties (e.g. Refs. [1–5] and references therein).

Correspondence to: J. Karger-Kocsis (karger@ivw.uni-kl.de).

Journal of Applied Polymer Science, Vol. 108, 2840–2851 (2008)

The tribological performance of thermoplastics and thermoset polymers with organoclay and CNT loadings became under spot of interest only recently.[6–9] The wear performance of rubbers containing the above-mentioned fillers was scarcely studied.[9,10] It has to be emphasized that the friction and wear parameters are system dependent ones, i.e. their values strongly depend on the related test configuration and testing parameters selected. Though the abrasion of rubbers was well studied, far less information is available on their sliding and rolling wear behaviors. Moreover, less attention was paid to the rolling friction and wear of rubbers after the pioneering works in the 50s.[11–15] On the other hand, the complex sliding/rolling movements during orbital rolling is an interesting tribotest to get further insight in the wear mechanisms of rubbers. As a consequence, the aims of this study were:

1. to study the dry sliding and rolling wear properties of a rubber containing multiwall carbon nanotube (MWCNT) filler and to collate the results with those formulations which contained silica filler,
2. to perform the tribotests in various test rigs, and
3. to deduce correlations between wear and mechanical properties.

As rubber a peroxide-cured hydrogenated acrylonitrile/butadiene rubber (HNBR) was selected. HNBR is preferred in many applications because of its outstanding oil- and temperature-resistance. It is the right place to mention that unlike to sliding wear, results on the abrasion wear of HNBR stocks are already available.[16]

EXPERIMENTAL

Materials

The composition of the peroxide curable HNBR was the following: HNBR (Therban® LT VP/KA 8882 of Lanxess, Leverkusen, Germany; acrylonitrile content: 21%, Mooney viscosity ML (1 + 4) 100°C = 74), 100 part; diphenylamine-based thermostabilizer (Luvomaxx CDPA of Lehmann & Voss, Hamburg, Germany), 1.1 part; zinc-containing mercapto-benzimidazole compound (Vulcanox® ZMB 2/C5 of Lanxess), 0.4 part, *t*-butylperoxy-diisopropyl benzene (Perkadox 14–40 B-PD of Akzo-Nobel, Düren, Germany; active peroxide content: 40%), 7.5 part; MgO, 2 part; triallyl isocyanurate, 1.5 part; ZnO, 2 part. This mix was produced separately and provided by Lanxess. The curing time of this base mix to reach 90% crosslinking was about 10 min at $T = 175$°C. This peroxide curable HNNBR was mixed with 10 and 30 parts per hundred rubber (phr) MWCNT (Baytubes® C 150 P from Bayer MaterialScience, Leverkusen, Germany) and with silica (Ultrasil® VN2 of Degussa, Frankfurt, Germany) fillers on a two-roll mixing mill (LRM-150BE of Labtech, Bangkok, Thailand) at about 40°C by setting a friction ratio of 1.5.

Curing of the silica and MWCNT filled HNBR to 2 mm thick sheets (100 × 100 mm^2 surface) occurred at $T = 175$°C for 15 min in a laboratory press. Specimens for the investigations listed below were cut/punched from these sheets.

The above fillers differ from one another markedly in respect to their chemical build-up and physical structure. Nevertheless, their tribological effects can be compared considering that both of them belong to the category of active rubber fillers.

Dispersion of the MWCNT

The disentanglement of the MWCNT was assessed by transmission electron microscopy (TEM). TEM images were taken from thin section of the rubber 10 phr MWCNT-containing HNBR using a Leo 912 Omega microscope (Oberkochen, Germany) with an accelerator voltage of 120 kV. The thin sections (ca. 100 nm) were cryo-cut with a diamond knife at about −120°C and used without staining.

Dynamic-mechanical thermal analysis

Dynamic-mechanical thermal analysis (DMTA) spectra were recorded on rectangular specimens (length × width × thickness = 20 × 10 × ca. 2 mm^3) in tension mode as a function of temperature (from −100°C to +100°C) and a frequency of 10 Hz using a Q800 device of TA Instruments (New Castle, DE). Tests were run at a constant strain (0.01%) by heating the specimens in a stepwise manner (temperature steps of 5°C were followed by an equilibration period of 3 min at each temperature).

Hardness and density

The Shore A hardness of the rubbers was determined according to ISO 868 using a hardness measuring device of Zwick (Ulm, Germany). The universal hardness (HU) was determined by the DIN 50359-1 standard using a Shimadzu DUH 202 device with a Vickers-type diamond indenter. During the microhardness measurements the maximum force and its holding time were 5 mN and 2 s, respectively. For the density determination the Archimedes principle (buoyancy method with water) was adopted according to the ISO 1183. The test rig with density measurement kit was adjusted to a Mettler AT261 (Giessen, Germany) microbalance.

Mechanical properties

Tensile tests were carried out on 2 mm thick dumbbells (type:S1 according to DIN 53504) on a Zwick 1445 (Ulm, Germany) universal testing machine at a deformation rate of 500 mm/min. From the related stress–strain curves apart from the ultimate properties, the stress values at 100 and 200% elongations (termed M-100 and M-200, respectively) were also read (ISO 37). To determine the tear strength the recommendation of the ISO 34-1 standard was followed, i.e. angle-type specimen with cut was subjected to 500 mm/min deformation rate.

Sliding and rolling friction and wear tests

Friction and wear characteristics were determined in pin (steel)-on-plate (rubber) (POP) configuration using a Wazau device (Berlin, Germany), in which a steel pin (100Cr6; arithmetical roughness, R_a, less than 1 μm) with a hemispherical tip of 10 mm diameter rotated along a circular path (diameter: 33 mm). The pin was pushed against the rubber plate with a given load. The following parameters were selected for this configuration: normal load, 2 N; sliding speed, 250 mm/s; duration, 1.5 h. Measuring both the normal and the friction force components via a torque load cell thereby the coefficient of friction (COF) values were calculated and monitored during the test.

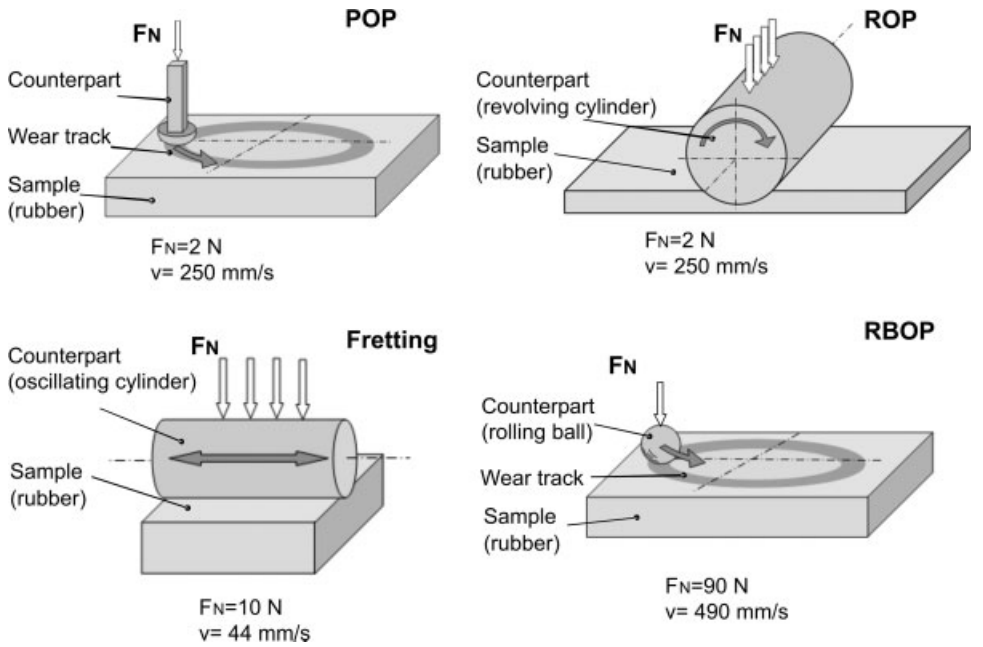

Figure 1 Schematic set-up of the tribotesting devices used. Designations: POP, pin (steel)-on-plate (rubber); ROP, roller (steel)-on-plate (rubber); Fretting, oscillating steel cylinder on rubber plate; RBOP, rolling ball (steel)-on-plate (rubber).

To study the sliding wear a further test, termed roller (steel)-on-plate (rubber) and referred to ROP, was also used. A rotating steel roller (100Cr6, diameter: 10 mm, width: 20 mm, $R_a \approx 0.9$ μm) pressed against a rubber strip of 9 mm width in a SOP 3000 tribotester (Dr Tillwich GmbH, Horb-Ahldorf, Germany). The frictional force induced by the torque was measured online and thus the COF was registered during the test. The test parameters were follows: load, 2 N; sliding speed, 250 mm/s; duration, maximum 1.5 h.

In the third tribotest (fretting) a steel cylinder was oscillating on the surface of the fixed rubber specimen. The cylinder was pressed against the rubber with a given load. The diameter and the contact length of the cylinder ($R_a \approx 0.9$ μm) were 15 and 12 mm, respectively. The applied normal load was 10 N, the frequency of the oscillation was 10 Hz, the stroke 2 mm, and the duration of the measurements was 3 h.

The rolling friction and wear behavior of the HNBR materials were investigated on a home built machine. On a fixed plate, covered by the rubber specimen, a steel ball was rolling along a circular path. The ball was driven by a rotating steel plate with a guiding groove when pressed against the specimen by a given load. The average diameters of the circular path and rolling ball (100Cr6 steel, $R_a \approx 0.9$ μm) were 33 and 14 mm, respectively. The applied load was 90 N, the speed was fixed at 483 mm/s, and the duration of the tests was 3 h. The evolved torque was measured and the COF was determined during the measurements.

The test configurations are depicted schematically in Figure 1. The testing parameters along with basic characteristics of the testing rigs are listed in Table I.

The specific wear rates were determined by eq. (1):

$$W_s = \frac{\Delta m}{\rho F L} \tag{1}$$

where Δm is the mass loss recorded gravimetrically, ρ is the density, F is the normal force, and L is the overall sliding distance.

TABLE I
Test Parameters and Basic Characteristics of the Tribotests Used

Tribotest configuration	Diameter of the counterpart (mm)	Contact length, L (mm)	Normal load, F_N (N)	Revolution number/ frequency	Radius/amplitude of the motion (mm)	Roughness of the counterpart
POP	10	–	2	144 rpm	16.5	$R_a = 0.9$ μm
ROP	10	8.5	2	137 rpm	–	$R_a = 1$ μm
Fretting	15	12	10	10 Hz	2	$R_a = 0.89$ μm
RBOP	14	–	90	280 rpm	16.5	$R_a = 0.89$ μm

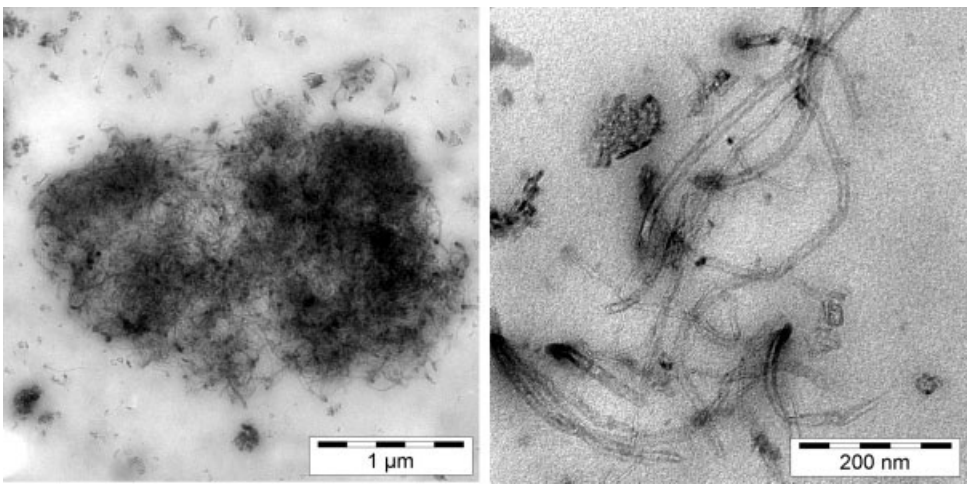

Figure 2 Characteristic TEM pictures showing the dispersion of MWCNT in the HNBR containing 10 phr MWCNT.

Wear mechanisms

Worn surfaces of the specimens were inspected in a scanning electron microscope (SEM; JSM5400 of Jeol, Tokyo, Japan). Prior to SEM investigation the specimens were sputtered with an Au/Pd alloy using a device of Balzers (Lichtenstein).

RESULTS AND DISCUSSION

HNBR characteristics

TEM pictures in Figure 2 indicate that the MWCNTs are not fully exfoliated, disentangled. One can find some large agglomerates of MWCNT, as well as well as some individually dispersed CNTs in the HNBPR + 10 phr MWCNT.

MWCNT outperformed the silica as reinforcement at the same filler loading based on the DMTA spectra (cf. Fig. 3). Figure 3(a) displays the change in the storage modulus, whereas Figure 3(b) the change in the mechanical loss factor (tan δ) as a function of both temperature and rubber composition. Comparing the related traces for the HNBR with 10 and 30 phr MWCNT and silica, respectively, one can clearly see the relative increment in the storage and relative reduction in the mechanical loss peak for MWCNT. Incorporation of MWCNT in 30 phr amount increased unexpected prominently the stiffness both in the glassy and rubbery stages of the HNBR [cf. Fig. 3(a)]. The most likely reason for this is breakage (fragmentation) of the MWCNTs owing to tube/tube interaction, attrition. By this way more and more MWCNT fragments can be ''wrapped'' by the rubber molecules and thus act as a ''stiff'' reinforcement of low aspect ratio. During the fragmentation process rubber may also be grafted onto the MWCNT surface. The overall effect of this scenario is a substantial reinforcing effect which should manifest also in the mechanical performance (see later). The glass transition temperature (T_g) was not influenced by

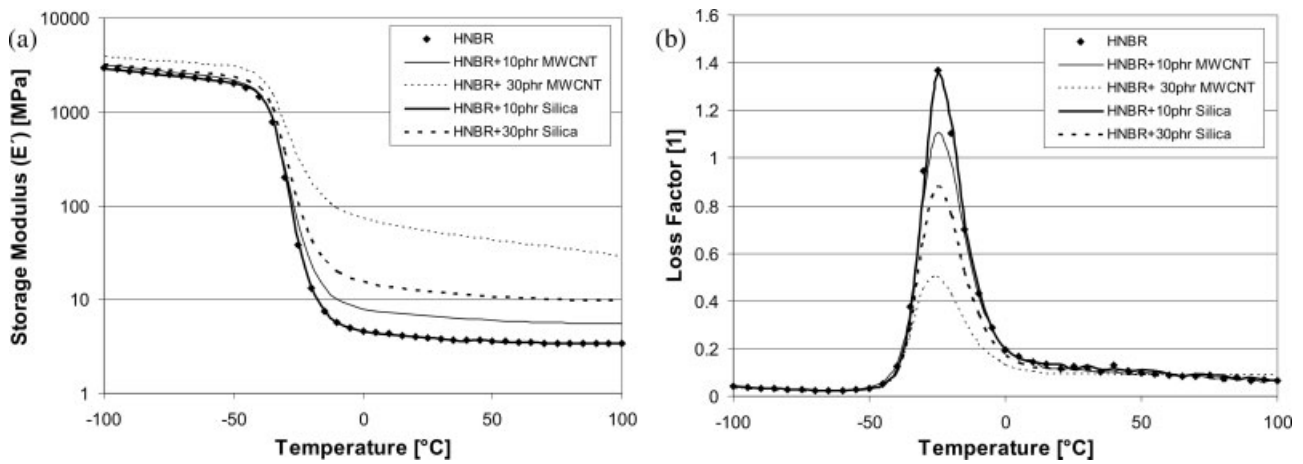

Figure 3 Storage modulus (a) and mechanical loss factor (b) as a function of the temperature for the HNBR mixes studied.

TABLE II
Network-Related and Mechanical Data for the HNBR Rubbers Containing MWCNT and Silica as Fillers

	Composition				
Property, unit	HNBR	HNBR + 10 phr MWCNT	HNBR + 30 phr MWCNT	HNBR + 10 phr silica	HNBR + 30 phr silica
M_c (g/mol)	1931	1113	150	1952	667
ν_c ($10^{+26} \times m^{-3}$)	3.3	5.7	45.3	3.3	10.3
tan δ at T_g (1) is the unit	1.36	1.1	0.5	1.34	0.88
Density (g/cm^3)	1.057	1.057	1.135	1.066	1.141
Shore A (°)	42	56	82	49	61
HU (MPa)	1.45	2.16	10.2	1.7	4.86
M-0.01 DMTA (MPa)	3.9	6.7	52.4	3.87	12.1
M-100 (MPa)	1.27	2.4	12.7	1.43	2.36
M-200 (MPa)	2.6	4.68	16.51	3	4.66
Tensile strength (MPa)	4.4	4.9	16.5	4.7	17.2
Tensile strain (%)	280	179	132	265	476
Tear strength (kN/m)	4.2	8.0	22.0	5.3	12.5

the type and amount of the fillers. According to the rubber elasticity theory, the inverse of the plateau modulus ($1/E_{pl}$) at a given temperature above T_g correlates with the mean molecular mass between crosslinks (M_c):

$$E_{pl} = \frac{3\rho RT}{M_c} \quad (2)$$

where E_{pl} is the modulus at $T = 293$ K, ρ is the density, R is the universal gas constant (8.314 J/(K mol), and T is the absolute temperature (i.e. $T = 293$ K).

Alternatively, the apparent crosslink density (ν_c) can be considered:

$$\nu_c = \frac{N\rho}{M_c} \quad (3)$$

where N is the Avogadro or Loschmidt number (6.023×10^{23} mol^{-1}).

It has to be emphasized that both M_c and ν_c are apparent values. They reflect not only the chemical crosslinking (which is likely constant for the HNBR recipes) but also the rubber–filler and filler–filler interactions. It is worth of noting that the very low M_c of HNBR + 30 phr MWCNT is attributed to the above mentioned reinforcing effect of the MWCNT fragments. The network-related data are summarized in Table II.

The Shore A and universal hardness (HU) values are also increasing with increasing MWCNT or silica contents. The M-0.01, M-100, M-200 values which are the moduli at 0.01 (read from the DMTA traces), 100, and 200% elongations (read from the tensile stress-strain curves) respectively, just like the tensile and tear strengths are also increasing with increasing filler content. The course of the ultimate tensile strain as a function of filler content differs for the MWCNT and silica, with increase in MWCNT content and the ultimate tensile strain decrease, whereas the opposite trend was found for the silica filler (after a small reduction compared to the neat HNBR at 10 phr silica content)—cf. Table II. The highest stiffness and strength data along with the lowest ductility for the HNBR + 30 phr MWCNT are in line with the suspected fragmentation of the latter. Note that this behavior is in strong analogy with discontinuous fiber reinforced thermoplastics when their properties are considered as a function of fiber content.

Comparison of the tribotesting conditions

The determination of the exact contact pressure during the measurements is very difficult because of the viscoelastic behavior of the rubber, progressing wear, and temperature development. However, with the selected normal loads the average contact pressures (σ_{Nave}) are similar in the beginning of the tests, at least for POP, ROP, and fretting. Note that during dry sliding the contribution of the interfacial wear

TABLE III
Average Normal Pressure (σ_{Nave}) Estimated for Different Tribotests by Adopting the Simplifications and Assumptions of the Hertzian Theory

Normal pressure, unit	Tribotest configuration	HNBR	HNBR + 10 phr MWCNT	HNBR + 30 phr MWCNT	HNBR + 10 phr silica	HNBR + 30 phr silica
σ_{Nave} (MPa) (running-in phase)	POP	0.49	0.71	2.82	0.49	1.06
	ROP	0.22	0.29	0.83	0.22	0.39
	Fretting	0.35	0.46	1.29	0.35	0.62
	RBOP	1.41	2.03	8.01	1.41	3.01

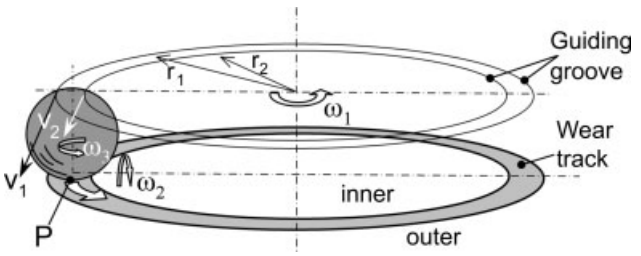

Figure 4 Kinematics of the rolling ball in the RBOP device.

(i.e. adhesion component) should be markedly larger than that of the hysteretic contribution.[17] On the other hand for the RBOP device, where hysteretic heating should dominate, a rather high normal load was needed to reach measurable wear (cf. Table III). The average sliding speeds of the steel counterparts compared to the fixed rubber specimens are the same for the POP, ROP, and fretting measurements. Such a sliding value (relative displacement) can hardly be defined when the steel counterpart is rolling, as it is the case for RBOP testing. Owing to the above aspects, results of the POP, ROP, and fretting tests will be shown together, i.e. separated from those of RBOP.

During the POP, ROP tests pure sliding appears between the steel counterpart and the rubber specimen. Although the relative sliding speed changes across the contact area, the sliding direction remains the same in every moment. During the fretting test, the direction of the relative displacement between the surfaces of the rubber and the steel counterpart is reciprocating.

In the RBOP tribotest device the steel ball is driven by the revolving guiding groove (cf. Fig. 4). At the contact points of the rotating (ω_1) grooved plate and the rolling ball different velocities evolve (V_1, V_2). This is because of the difference in the radii of the groove by keeping the ball in trace (r_1, r_2). The velocity difference $V_1 - V_2$ generates a spinning motion of the ball (ω_3) [cf. Figs. 4 and 5(a)]. At the same time, the velocity difference between the upper side (contact with the edges of the rotating guiding groove) and the bottom side (contact with the fixed rubber specimen) of the ball induces a forward rolling (ω_2) [cf. Figs. 4 and 5(b)]. Because of the additional spinning motion, a rotation sliding occurs at the contact ellipse where the sliding speed changes. The elliptical contact surface is due to the fact that the ball rolls in the wear track of the rubber. The maximal value of this sliding component is noted by $V_{3\text{max-slide}}$ [cf. Fig. 5(a)]. During the forward rolling the ball ''sticks'' are at the bottom point (pole point ''P'') of the ball. On the basis of the works of Heathcote (see in Refs. 12 and 18) this sliding zone is complex in respect with the relative displacements. It contains zones both with forward and backward sliding motions [cf. Fig. 5(b,c)]. If we assume a perfect sticking in the point ''P,'' the maximal value of this sliding speed [$V_{2\text{max-slide}}$ in Fig. 5(c)] correlates with the indentation depth of the ball (i.e. depth of the wear groove).

On the basis of the geometry-related calculations and assumptions about the indentation we have got: $V_{2\text{max-slide}} \approx 0.33 V_{3\text{max-slide}}$. The superposition of the two different sliding fields [Fig. 5(a,c)] informs us about the local sliding directions and estimated relative velocities in the contact area (cf. Fig. 6). Consequently, at the outer side of the contact area the relative sliding speed of the ball against the rubber is larger than at the inner side of the track. The direction of the sliding in the outer side is forward whereas at the inner side it is backward. The SEM pictures taken from the neat HNBR rubber after RBOP test seem to verify this theory (see later).

The estimated average normal pressures (σ_{Nave}), arising when pressing different steel counterparts against the flat rubber specimens, are summarized in Table III. It is noteworthy that the normal pressure values, estimated by the Hertzian theory, change with the temperature and also with wear history (the latter obviously affects the width and depth of the worn surface). Nevertheless, these results are still usable to compare the test conditions. Note that the σ_{Nave} data are far below those of tensile and tear strength values of the corresponding rubbers (cf. Table II). With increasing hardness (stiffness) of the

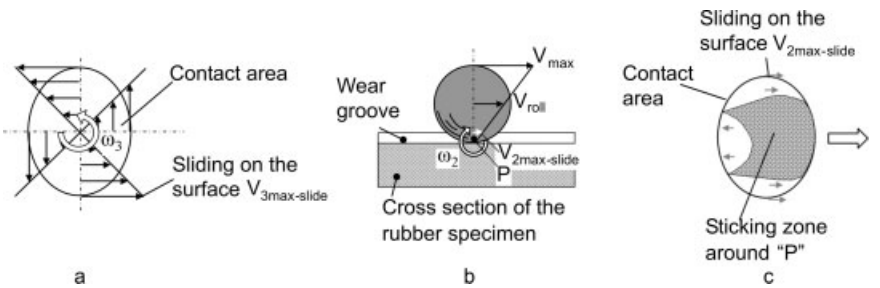

Figure 5 Sliding directions at the elliptic contact area of the steel ball and the rubber specimen caused by the spinning-ω3 (a) and rolling motions-ω2, (b), a schematic sketch of the forward rolling of the ball in the groove is given in picture (c) shows the contact surface at forward rolling.

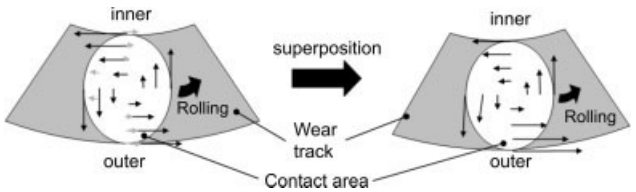

Figure 6 Superposition of the sliding velocities in the contact area during orbital rolling.

rubber the computed average normal pressure data also increases. For the related calculations the M-0.01 moduli (cf. Table II) of the rubbers were used. Attention requires the fact that for the RBOP tests the estimated normal pressure values are much higher than for the other tribotests (cf. Table III).

Coefficient of friction

Figure 7 indicates the effects of MWCNT and silica on the COF. One can recognize that the COFs are in the same range in POP and fretting tests, while the COF is markedly higher for the ROP configuration. This is due to the related test set-up of ROP favoring substantial heating of the specimen and the consequence of which may be rubber against rubber (when the roller is coated with rubber) type friction. As expected, in RBOP testing the COF is about one order of magnitude smaller than for the other tribotests [cf. Fig. 7(a,b)]. Moreover, the change in the COF with the MWCNT and silica contents is different when various test devices are used. For the POP configuration, the COF is increasing with increasing MWCNT or silica contents as compared to the neat HNBR [cf. Fig. 7(a)].

Using the ROP device the measured COF of HNBR became smaller when MWCNT was added, and with increasing MWCNT content the COF decreased. If HNBR is filled with silica, the COF is higher than that of the neat HNBR, but its value decreases with the silica content. During fretting the observed COF was always higher than the neat HNBR irrespective of either MWCNT or silica was incorporated. However, with increasing filler content the COF values during fretting slightly decreased [cf. Fig. 7(a)]. For the RBOP tests the measured COFs slightly increased compared to the neat HNBR. Moreover, with increasing filler content the COF increased as well [cf. Fig. 7(b)].

Specific wear rate

Comparing the specific wear rates one can see that their differences may cover several order of magnitudes [cf. Fig. 8(a,b)]. The largest wear is caused by the POP tests, the smallest one by the RBOP tests. Using MWCNT or silica additives the wear resistance of the related HNBR mixes, compared to that of the pure HNBR, was mostly enhanced. This tendency did not hold, however, for the HNBR + silica systems in fretting and for the HNBR + 10 phr silica in RBOP tests. One can also recognize that at the same filler loading MWCNT bestows a better wear resistance than silica. With increasing filler content the resistance to wear of the HNBR compound is usually enhanced. This is not valid for the ROP tests of the HNBR + silica systems [cf. Fig. 8(a)] where the wear rate increased with increasing silica content. It should be born in mind that the specific wear rate is usually decreasing with increasing active filler content as demonstrated for carbon black.[19,20]

Wear mechanisms

Characteristic SEM pictures taken for the worn tracks of the HNBR stocks are displayed in Figures 9 and 10 for the POP and ROP tests, respectively.

POP tests

The surface of the evaluated wear track on the pure HNBR shows that quite large particles were chipped

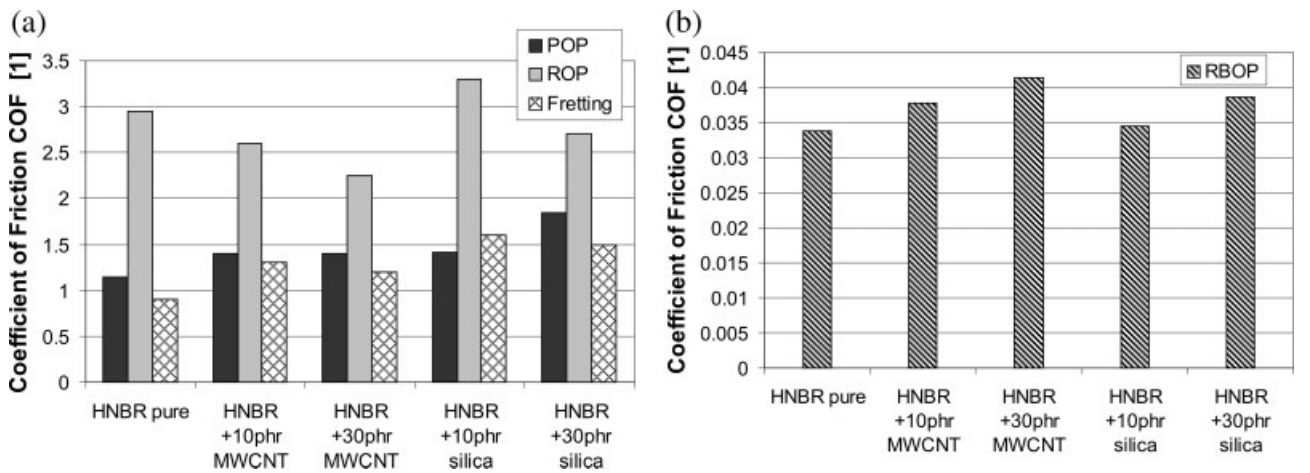

Figure 7 Measured steady-state COF values for the POP, ROP, and fretting (a), as well as for the RBOP tests (b).

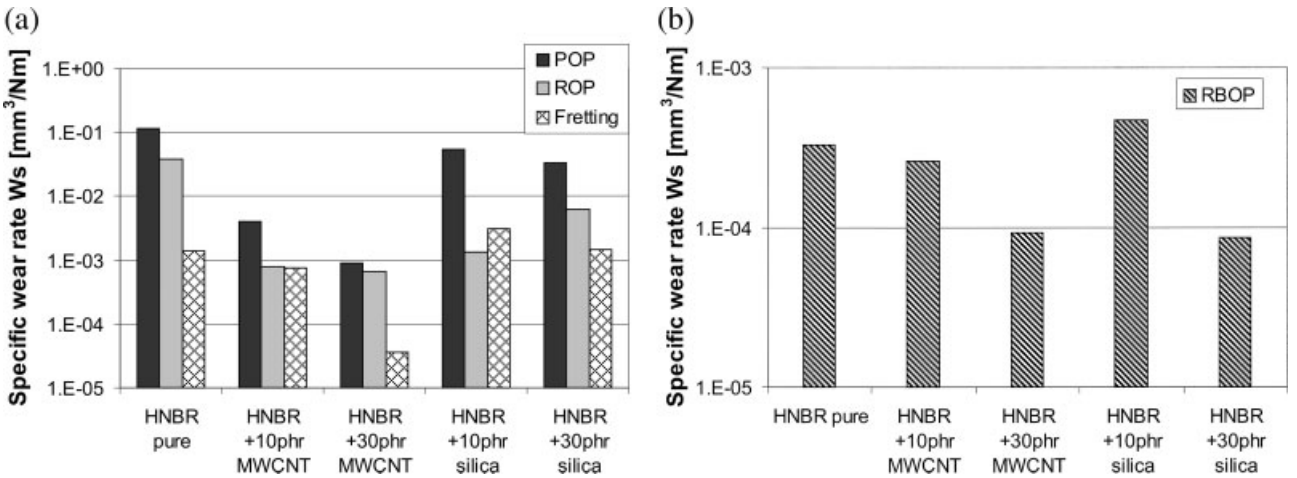

Figure 8 Specific wear rate data for the POP, ROP, and fretting (a), as well as for the RBOP tests (b).

off from the surface and a crater-like pattern appeared [Fig. 9(a)]. At 10 phr MWCNT content, however, the so-called Schallamach waviness[21,22] becomes recognizable [Fig. 9(b)], with further increase of the MWCNT content the Schallamach waves become less resolved and a band-like pattern appeared [Fig. 9(c)]. The reason of the latter may be linked with the MWCNT fragments inducing the discussed reinforcing effect. Another effect that may be at work is the radical scavenging guaranteed by the MWCNT. Nevertheless, the smooth worn surface suggests low wear that was found in fact [cf. Figs. 8(a) and 9(c)]. Interestingly, the smooth surface appearance was not accompanied with low COF in this case [cf. Fig. 7(a)]. When 10 phr silica was added to the HNBR spherical debris along with Schallamach waves, oriented perpendicular to the sliding direction, were observed in the wear track after the POP test [Fig. 9(d)]. With increasing silica content (to 30 phr) the wear mechanisms changed: large debris agglomerates appeared and the Schallamach waves disappeared [Fig. 9(e)].

ROP tests

On the worn surface of the pure HNBR chipped off debris, roll formation and spherical particles are seen [Fig. 10(a)]. This suggests that high COFs [cf. Fig. 7(a)] and wear rates [cf. Fig. 8(a)] were found in fact. By reinforcing the HNBR with 10 phr MWCNT, the worn surface becomes smeared [Fig. 10(b)] indicating the lower COF and Ws in accordance with the experimental findings. With increasing MWCNT content (30 phr) the surface of the wear track become ever smoother, and practically no wear debris or cracks could be found [Fig. 10(c)]. In that case the MWCNT worked as an internal lubricant at the same time. If the HNBR contained 10 phr silica, extended rolls appeared on the surface perpendicular to the sliding direction after the ROP tests [Fig. 10(d)]. With increasing silica filler content the density of the rolls decreased and the surface become smoother (''ironed'') [cf. Fig. 10(e)]. In this case the ''smeared'' (ironed) surface is probably the effect of thermal decomposition which has been reported for several types of rubbers by Gent and Pulford.[23] As suggested earlier, the thermal decomposition could be efficiently reduced when MWCNT acts as radical scavenger.

Fretting tests

The worn surfaces showed pronounced similarities with those of the ROP tests and thus they are not treated separately in this article.

RBOP tests

The analysis of the wear tracks after RBOP tests is far more difficult than for the other tribotests. Because of the peculiar motion of the rolling ball, the wear track should be separated into three regions namely outer-, middle-, and inner-side [Fig. 11(a)]. The SEM pictures in Figure 11 are selected at different magnifications in order to demonstrate characteristics of the related failure modes. The superimposed sliding and rolling motions of the ball were treated in detail before (cf. Figs. 4–6). Note that the sliding direction is downwards at the outer side, and upwards at the outer side, as shown by arrows at the related SEM pictures. For the pure HNBR rubber Schallamach type waviness can be found both in the outer and inner sides of the wear track. In the middle section rolled debris can be observed. The Schallamach type waves are especially well-developed in the outer side [Fig. 11(b)]. When 10 phr

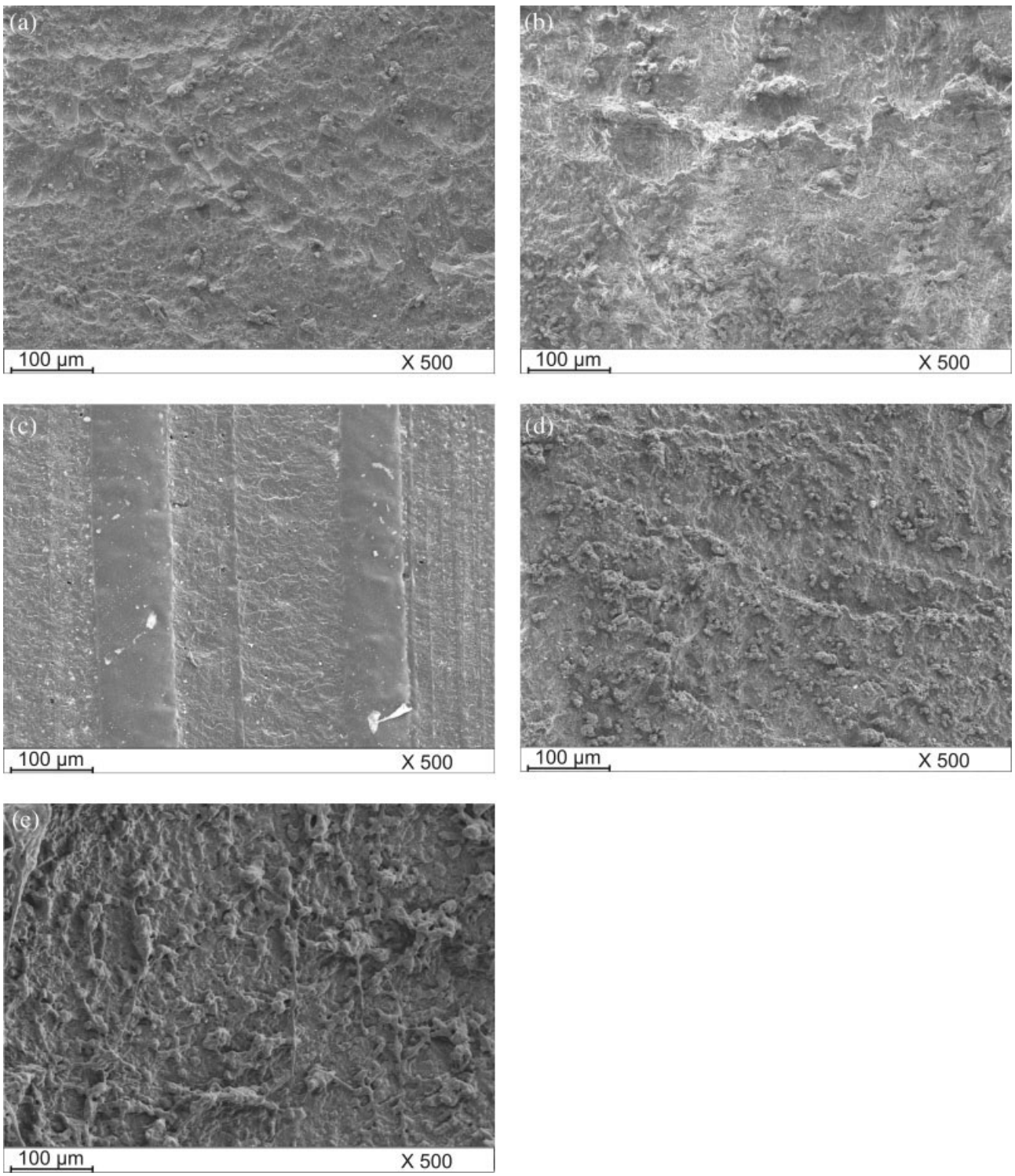

Figure 9 SEM pictures taken from the wear tracks after POP tests (a) pure HNBR, (b) HNBR + 10 phr MWCNT, (c) HNBR + 30 phr MWCNT, (d) HNBR + 10 phr silica, and (e) HNBR + 30 phr silica. Note: sliding directions is downwards.

MWCNT was added to the HNBR, the scenario changed. The onset of Schallamach type waves and debris deposition are still characteristic for the outer side and for the middle regions, respectively, but no wave formation can be recognized in the inner side. The surface of the inner side is produced by chipping [Fig. 11(c)]. At 30 phr MWCNT content in the outer side small sized debris can be found on the surface. In the middle region dense waviness, offset to the rolling direction, can be resolved. At the inner

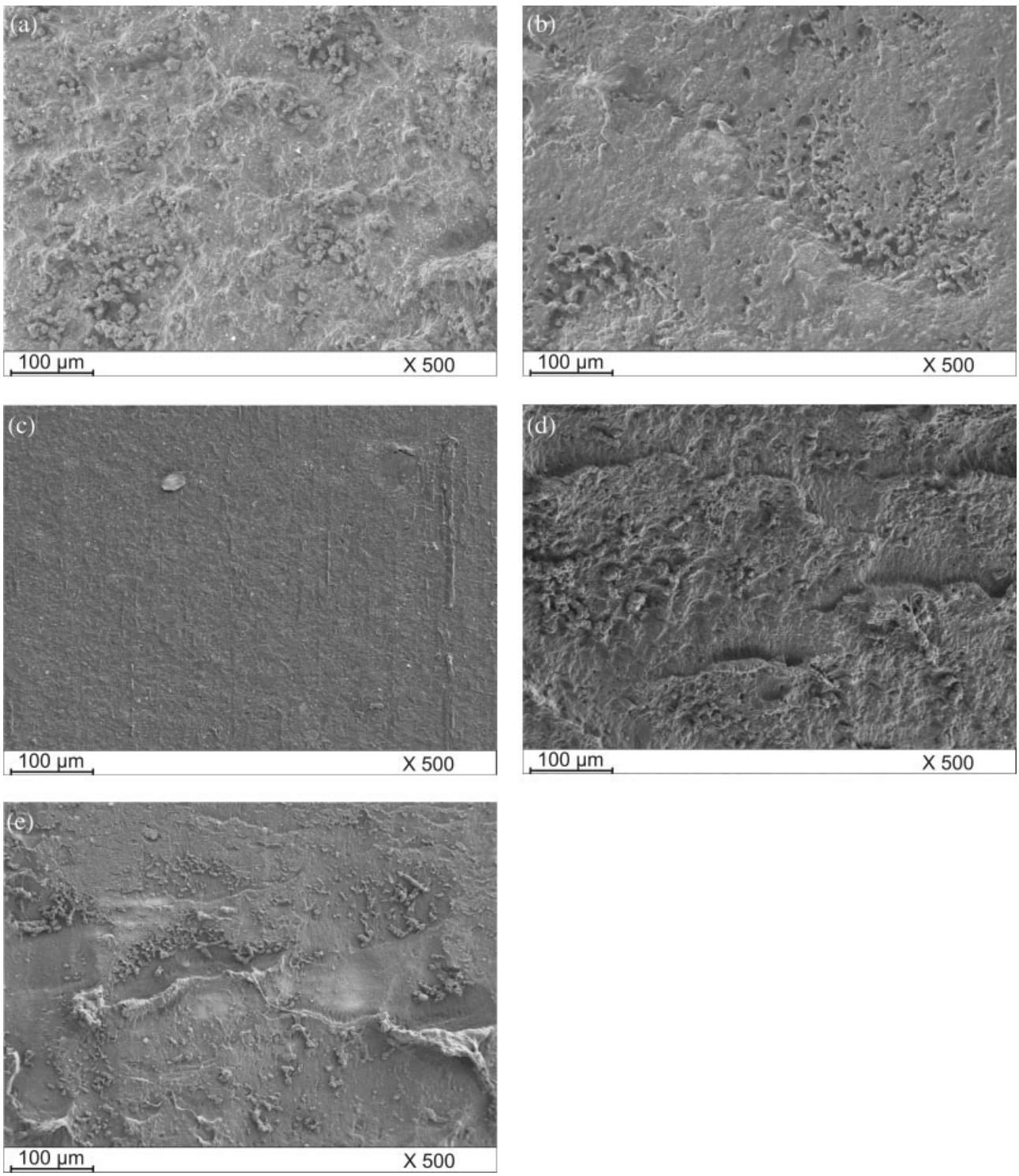

Figure 10 SEM pictures taken from the wear tracks after ROP tests (a) pure HNBR, (b) HNBR + 10 phr MWCNT, (c) HNBR + 30 phr MWCNT, (d) HNBR + 10 phr silica, and (e) HNBR + 30 phr silica. Note: sliding directions is downwards.

side of the track somewhat larger particles than in the mid section appeared [Fig. 11(d)]. When the HNBR contained 10 phr silica, Schallamach-type waves appeared both in the outer and at the inner sides of the track. In the middle region rolls formed which were deposited in offset direction to that of the rolling [Fig. 11(e)]. With increasing silica content the HNBR failed by formation of spherical debris. One can see that the particle size becomes finer when moving from the outer towards the inner part

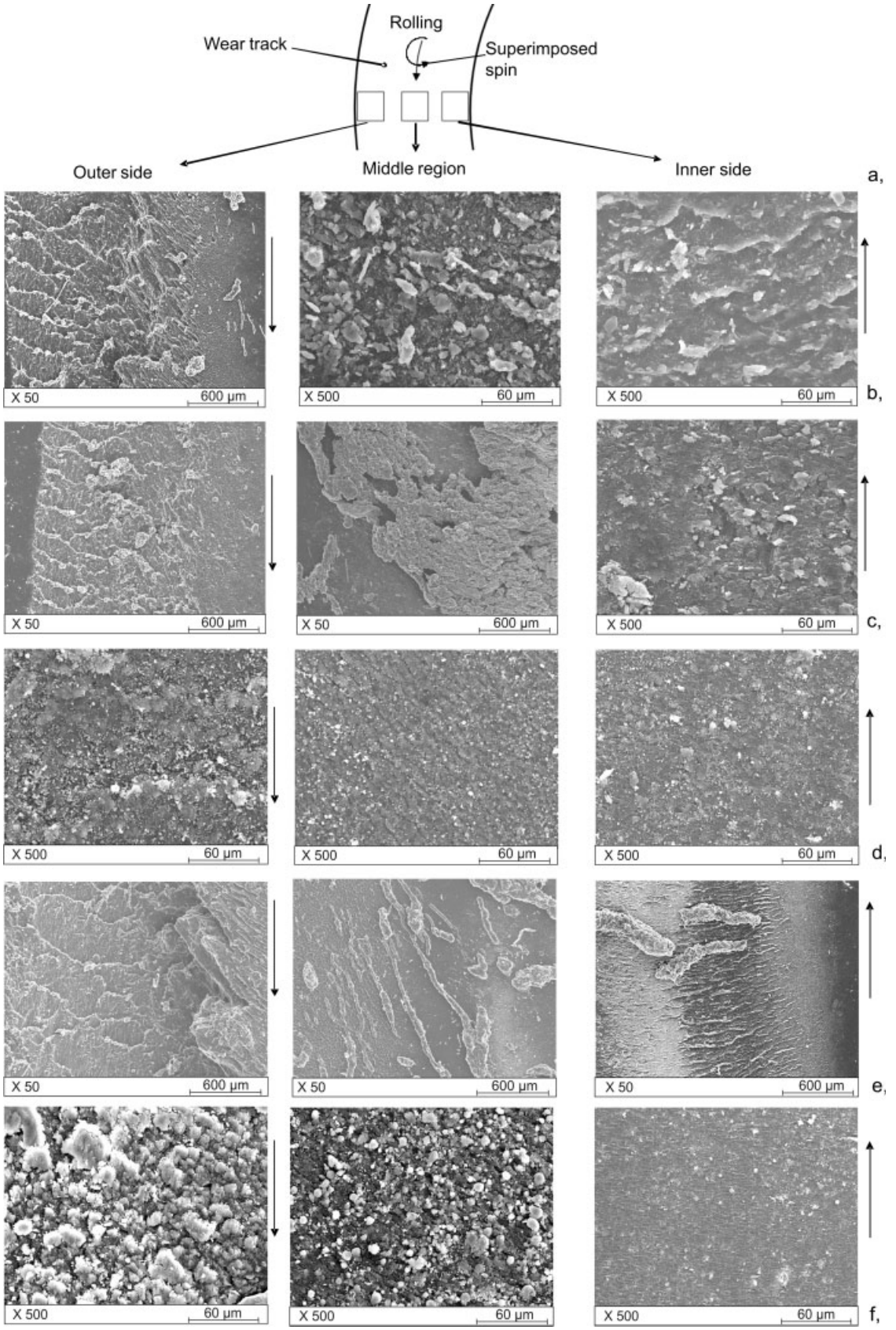

Figure 11 SEM pictures taken from the wear tracks after RBOP tests (a) explanatory overview on the wear track, (b) pure HNBR, (c) HNBR + 10 phr MWCNT, (d) HNBR + 30 phr MWCNT, (e) HNBR + 10 phr silica, (f) HNBR + 30 phr silica.

of the worn track. At the inner side of the wear track small and dense cracks perpendicular to the sliding direction can also be resolved [Fig. 11(f)].

CONCLUSION

The aim of this study was to investigate the mechanical and tribological properties of a peroxide cured HNBR material with different MWCNT and silica particle contents and to collate the results. On the basis of this work the following conclusions can be drawn:

1. It has been established that with increasing filler content the hardness, the tensile and tear strengths, and the apparent crosslinking density increased. The ultimate tensile strain decreased with increasing MWCNT content but increased with increasing silica content. The improvement in the tensile strength did not depend on the type of the filler in the HNBR. By contrast, the upgrade in the tear strength was markedly higher for MWCNT than for silica fillers. Unlike silica, the ultimate tensile strain was markedly reduced with increasing MWCNT content. This was attributed the reinforcing effect of MWCNT fragments. The apparent crosslinking density was also higher for MWCNT than for silica when incorporated in the same amount in the HNBR.
2. Values of the COF proved to be highly dependent on the testing rigs (''system parameter''). Nevertheless, the COF seems to increase when the studied fillers are incorporated in HNBR.
3. From the viewpoint of wear resistance MWCNT is a much better filler than silica. It should be emphasized again that the observed improvement in the specific wear rate strongly depends on the configuration of the tribotests. Increasing filler content enhanced the resistance to wear. This is in line with findings reported for the tribological effect of increasing carbon black content in rubbers.
4. Between the mechanical and tribological properties of the investigated HNBR systems no definite correlations can be traced. The complexity of the wear behavior requires a large data base in respect with the thermo-mechanical and network-related properties of rubbers in order to find such correlations, if any.

The authors are thankful to Mr. G. Mencia and to Mrs. N. Marinova (IVW Kaiserslautern Germany) for their involvement in the fretting and POP and ROP tests, respectively. The authors thank Dr. R. Thomann (Freiburg, Germany) for the TEM study. This work was performed in the framework of an integrated project of the EU (KRISTAL; Contract Nr.: NMP3-CT-2005-515837; www.kristal-project.org).

References

1. Utracki, L. A. Clay-Containing Polymeric Nanocomposites; Rapra Technology: Shawbury, UK, 2004.
2. Karger-Kocsis, J.; Zhang, Z. In Mechanical Properties of Polymers Based on Nanostructure and Morphology; Michler, G. H.; Baltá-Calleja, F. J., Eds.; CRC Press: Boca Raton, FL, 2005; Chapter 13, p 553.
3. Zheng, H. C. In Handbook of Organic–Inorganic Hybrid Materials and Nanocomposites; Nalwa, H. S., Ed.; American Scientific Publ: Los Angeles, CA, 2003; Vol. 2, Chapter 4, p 151.
4. Maiti, M.; Bhowmick, A. K. J Appl Polym Sci 2007, 105, 435.
5. Du, J.-H.; Bai, J.; Cheng, H.-M. Express Polym Lett 2007, 1, 253.
6. Xue, J.; Wu, W.; Jacobs, O.; Schädel, B. Polym Test 2006, 25, 221.
7. Burris, D. L.; Boesl, B.; Bourne, G. R.; Sawyer, G. Macromol Mater Eng 2007, 292, 387.
8. Chen, H.; Jacobs, O.; Wu, W.; Rüdiger, G.; Schädel, B. Polym Test 2007, 26, 351.
9. Karger-Kocsis, J.; Felhös, D. In Tribology of Polymeric Nanocomposites; Friedrich, K.; Schlarb, A. K., Eds.; Elsevier: Amsterdam; to appear.
10. Gatos, K. G.; Kameo, K.; Karger-Kocsis, J. Express Polym Lett 2007, 1, 27.
11. Eldredge, K. R.; Tabor, D. Proc R Soc London Ser A 1955, 229, 181.
12. Tabor, D. Proc R Soc London Ser A 1955, 229, 198.
13. Flom, D. G.; Bueche, A. M. J Appl Phys 1959, 30, 1725.
14. Grosch, K. A. Rubb Chem Technol 1996, 69, 495.
15. Gent, A. N.; Gallagher, D. D.; Steven, R. B. Polym Eng Sci 2007, 47, 1576.
16. Thavamani, P.; Bhowmick, A. K. J Mater Sci 1993, 28, 1351.
17. Briscoe, B. J.; Shina, S. K. In Wear—Materials, Mechanisms and Practice; Stachowiak, G. W., Ed.; Wiley: New York, 2005; Chapter 10, p 223.
18. Halling, J., Ed. Principles of Tribology; Macmillan Press: London, 1975; Chapter 8, p 182.
19. El-Tayeb, N. S. M.; Nasir, R. Md. Wear 2007, 262, 350.
20. Karger-Kocsis, J.; Mousa, A.; Major, Z.; Békési, N. Wear 2008, 264, 359.
21. Schallamach, A. Wear 1957, 1, 387.
22. Schallamach, A. Wear 1971, 17, 301.
23. Gent, A. N.; Pulford, C. T. R. J Appl Polym Sci 1983, 28, 943.